

29A NASA-TM-X-55813 29B

3 A MAGNETIC CORE DIGITIZED SPARK CHAMBER FOR SPACE SCIENCE EXPERIMENTS 6

6 C. H. EHRMANN
C. E. FICHEL
D. A. KNIFFEN
R. W. ROSS 9

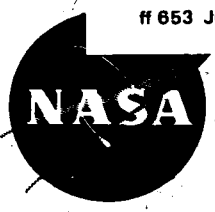
GPO PRICE \$ _____

CFSTI PRICE(S) \$ _____

Hard copy (HC) 3.00 9 JUNE 1967 10

Microfiche (MF) .65

ff 653 July 85



NASA

GODDARD SPACE FLIGHT CENTER

GREENBELT, MARYLAND 3

N67-29990

FACILITY FORM 802
(ACCESSION NUMBER)
1030RS
(PAGES)
TMX-55813
(NASA CR OR TMX OR AD NUMBER)

(THRU)
1
(CODE)
09
(CATEGORY)

1734

X-611-67-267

A MAGNETIC CORE DIGITIZED SPARK CHAMBER
FOR SPACE SCIENCE EXPERIMENTS

C. H. Ehrmann
C. E. Fichtel
D. A. Kniffen
R. W. Ross

June 1967

Goddard Space Flight Center
Greenbelt, Maryland

A MAGNETIC CORE DIGITIZED SPARK CHAMBER
FOR SPACE SCIENCE EXPERIMENTS

C. H. Ehrmann, C. E. Fichtel, D. A. Kniffen, and R. W. Ross

NASA/Goddard Space Flight Center
Greenbelt, Maryland

Abstract

A magnetic core digitized spark chamber suitable for use on balloons and ultimately on satellites has been developed. The assembled spark chamber consists of 32 active spark modules and forms the heart of a gamma-ray telescope. The individual modules consist of two orthogonal wire grids which form the spark chamber electrodes. Inclusion of a terminating resistor on each wire localizes the effect of the discharge, resulting in good multiple spark efficiency at low overvoltages. The lower voltages result in better spatial resolution with fewer wires sharing the spark. In the construction, considerable care was given to strength and long term operation under satellite conditions. The on-board data-handling system consists of a buffered memory readout, a housekeeping multiplexer, a tape recorder and a telemetry encoder and transmitter.

PRECEDING PAGE BLANK NOT FILMED.

CONTENTS

	<u>Page</u>
Abstract	i
Introduction	1
Selection of the detector	1
Single spark chamber module	3
Assembled spark chamber	7
Coincidence-anticoincidence system	8
The high voltage pulser	9
On-board data handling system	10
Concluding remarks	12
References	13
Figure captions	15

1. Introduction

The magnetic core digitized spark chamber described in this article was developed as a first step toward a much larger automatic spark chamber suitable for use on balloons and satellites. The detector described here is the heart of a celestial gamma-ray balloon experiment which has been flown many times in an oriented gondola. The basic problems associated with a spark chamber used in space applications are quite different from those used with particle accelerators. In the former, a spark chamber must be able to operate for a long time without renewing the gas, withstand shock, vibration, and large temperature extremes, be a true pressure tight system, be able to operate with the limited power available, and operate in close proximity to other electronics systems without interfering with their operation. On the other hand, the problems associated with very high count rates, which require fast circuitry, clearing fields, and very high data rate handling capability are not encountered.

In the following paragraphs we shall describe briefly the reasons for selecting a magnetic core digitized spark chamber for a particular experiment, since in part this discussion will show the value of this detector system. In the subsequent sections the detector will be described in detail, starting with the discussion of a single module and the relative merits of the possible approaches. This will be followed by a discussion of the whole assembly, the coincidence-anticoincidence circuit, the high voltage pulser and the data readout and handling system.

2. Selection of the detector

In the gamma-ray energy region chosen for examination in this experiment, 30 to 500 MeV, the dominant process lending itself to the detection and study of

energetic photons, as shown in Fig. 1, is pair-production. Since the measurement is to be made in a very high background of charged particles as well as a significant background of neutral induced events and albedo gamma-rays, a picture-type detecting apparatus is needed to identify unambiguously the pair-production event and to study its properties. There are presently four types of imaging devices which might be considered: the cloud chamber, bubble chamber, nuclear emulsion, and the spark chamber.

The cloud chamber and bubble chamber are not readily adaptable to space flight though one cloud chamber electron experiment has been flown successfully on balloons¹). Both of these types of detectors are heavy, bulky and very sensitive to the environmental extremes encountered in space flight. More significant is the excessive dead time in both cases and the lack of trigger capability in the bubble chamber. The nuclear emulsion has been used with some degree of success in gamma-ray astronomy in several experiments²⁻⁶), but this device lacks time resolution, being continuously sensitive from the time of manufacture until processing. This results in a large background of both charged particles and gamma-ray induced pairs, making the nuclear emulsion suitable only for searching for point sources and then only when the total background rate is sufficiently low. In addition to the background radiation problem, the data reduction time eliminates the nuclear emulsion technique for astrophysical gamma-ray studies unless it is used in conjunction with some sort of device to assist in locating the desired events.

The remaining imaging detector presently available for application to space research is the spark chamber. A spark chamber in principle can meet all of the requirements of a good gamma-ray detector. It can provide a pictorial image of

the pair-productions and, hence, provide an adequate means of discriminating against events which might themselves masquerade as gamma-rays. Spark chambers can be built in large modules thereby offering the possibility of constructing a detector system with the large area and solid angle needed for the study of the weak astrophysical gamma-ray sources. By using thin pair production plates between the individual spark chamber decks and using many spark levels, the direction of the primary gamma-ray can be determined within about 2° or better depending on energy, and the energies of the electrons can be estimated in the low energy region by multiple coulomb scattering. Time resolution is also available thereby permitting the selection of events formed during the useful portion of an exposure.

There are also several advantages of a digitized spark chamber over an optical one. These include: (1) no need for cameras or film reels, or for electronic image intensifiers or converters, (2) no film recovery or storage necessity, (3) direct binary data format with built-in storage and readout capability and no analog-to-digital conversion with its extraneous expansion of bit rate, and (4) low power drain because of the lack of a need for a high current spark and large spacing between active planes, (5) data immediately available in digital form for subsequent computer analysis. The gamma ray telescope as a whole is shown diagrammatically in Fig. 2.

3. Single spark chamber module

The fundamental approach to digitizing the spark chamber in the case discussed here is to replace an active plate with a wire grid, each wire of which is fed through a magnetic core which is set by the current in the wire associated with a spark. This technique has been discussed by Krienen^{7,8}) and Fischer,

et al.⁹). A series of different types of basic spark chamber units was tested in an effort to develop as satisfactory a system as possible.

The most desirable results were obtained using a module in which two orthogonal wire grids formed the spark chamber electrodes. This concept provides the capability of localizing the effect of the discharge, thereby achieving good multiple spark efficiency without the need for large overvoltages. The lower operating voltage results in better spatial resolution with fewer wires sharing the spark.

A module of the spark chamber that is used is shown in Fig. 3. The active area is 15.2 cm by 15.2 cm, and the wire grid consists of 128 parallel 0.18 mm diameter beryllium-copper wires, placed slightly less than 1.2 mm apart within the grid plane. The orthogonal grid planes are 2.24 mm apart (wire center to wire center).

Each wire is held under 5.6×10^5 dynes tension and ultrasonically welded and soldered to copper pins imbedded in terminal strips which are epoxied to the frame. This procedure solves the problem of accurate spacing of the wires, maintains a level wire plane, avoids undesired heating during the initial wire attachment, and provides an adequately strong bond. Beryllium-copper wire was used because of its tensile strength, toughness, and electrical conductivity. Careful selection of the actual wire used is needed to avoid kinks and coil hysteresis. The frames are machined from glass bonded mica, which is chosen for its low outgassing properties, in an attempt to minimize gas contamination during long term operation, without the need for flowing gas. This choice of material is also based on considerations of flexing strengths, tensile modulus, coefficient of thermal expansion, electrical insulation, and economy of fabrication. On the

high voltage grid, at one terminal strip the wires are terminated at the pins; while, at the other, the wire continues past the pin, is passed through the ferrite memory core, and is then attached to one side of a resistor R_w whose other end is attached to the common high voltage buss. On the grounded grid, the resistor is omitted and the buss is placed at ground potential. A detailed discussion of the mechanical engineering problems associated with the construction of these spark chamber modules is given by O'Conner ¹⁰).

Figs. 4 and 5 show results related to efficiency and spark spreading obtained in tests at a series of applied voltages and pressures using an R_w value of zero and 100 ohms respectively. It is clear that for a given pressure, the applied voltage should be maintained just slightly above the efficiency knee at the beginning of the plateau, since spark spreading is an increasing function of applied voltage. The tests also indicated that R_w can be chosen sufficiently large, namely about 100 ohms, to ensure a high multiple efficiency without seriously increasing the spreading.

The equivalent charging circuit is shown in Fig. 6. Analyzing this idealized circuit, a reasonable approximation to the high voltage profile as a function of time can be derived and is given by

$$V_p(t) = \frac{V_a}{C_p R_\ell} \left\{ \frac{1}{\alpha_- - \alpha_+} (e^{-\alpha_+ t} - e^{-\alpha_- t}) \right\}$$

where

(1)

$$\alpha_{\pm} = \frac{1}{2} \left[\left(\frac{R_\ell + R_0}{R_0 R_\ell C_0} + \frac{1}{R_\ell C_p} \right) \pm \sqrt{\left(\frac{R_\ell + R_0}{R_0 R_\ell C_0} + \frac{1}{R_\ell C_p} \right)^2 - \frac{4}{R_\ell R_0 C_0 C_p}} \right].$$

V_a is the high voltage applied to the anode of the pulser tube, V_p the resultant voltage appearing on the grid, and C_p is the measured capacitance of the module.

Some calculated voltage profiles for typical operating parameters are shown in Fig. 7 which shows the usefulness of a series resistor, R_ℓ , for adjusting the resultant peak grid voltage. The observed curves are similar to these except for a slight amount of ringing because of series inductances not taken into account in the idealized circuit.

R_w is neglected in the simplified charging circuit since the parallel combination of 128 of these resistors has a negligible effect on the voltage pulse shape, but they play a very important role during the spark discharge in serving to increase multiple spark efficiency. A possible inefficiency in recording all tracks when more than one is present arises because of the random fluctuation or jitter in spark formation time. Using the time jitter calculations of Schneider¹¹⁾ and the average observed spark formation time for this configuration of about 60 nanoseconds, the mean jitter time is 9 nanoseconds. Hence, the decay time, given approximately (assuming $R_\ell \ll R_w$) by

$$\tau_d = (C_0 + C_p) \frac{R_0 R_w}{R_w + R_0} , \quad (2)$$

must be large compared to 9 nanoseconds. With these considerations in mind, and for $C_p = 175$ pf, the measured value for the unit described here, the following parameter values were selected: $C_0 = 1000$ pf, $R_w = 100$ ohms, $R_0 = 150$ ohms, giving a decay time of about 70 nanoseconds.

Using a wire grid as the high voltage plane gives rise to a potential problem area. The high voltage is applied to a common buss from which wires pass through the ferrite memory cores and go on to the grid plane. Two additional wires, at ground potential, which are the reset and sense wires also pass through

each core. Good insulation in the core region is, therefore, essential to avoid circuit component failures resulting from high voltage breakdown.

The spark chamber gas being used is composed of a commercially available spark chamber gas which is 90% neon and 10% helium to which has been added 1% of argon for the Penning¹²) effect and 1/2% ethanol to suppress satellite sparking. Tests have shown that alcohol in percentages from 1/2 to 1% reduces satellite sparks, but larger percentages reduce the spark formation efficiency significantly. Because the orthogonal wire grids were only 2.24 mm apart, a gas pressure of 1.5 atmospheres was used to obtain a satisfactory efficiency.

4. Assembled spark chamber

The fully assembled spark chamber shown in Fig. 8 consists of 32 active spark modules and 30 pair converting plates divided into two identical spark chamber units of sixteen spark modules and fifteen plates each. The two units are stacked one above the other and separated by a thin (4.78 mm) 12.7 cm diameter circular Pilot B plastic scintillator which is used as one element of the triggering telescope. In each of the sixteen module units, all but the bottom module are the orthogonal (x-y) wire grid type described in the previous section. Because of the ambiguity of properly associating two or more x readings with the corresponding y readings, the bottom module in each unit contains wires arranged at 45 degrees with respect to the wires in the remainder of the modules. A metal plate is used as the ground electrode in these modules.

The pair converting plate between each module is .02 radiation length of gold plated on a structural layer of .18 mm (.002 radiation lengths) of aluminum. The use of many thin converters has the advantage of allowing an observation of the

created pair near the apex, prior to their passage through large amounts of scattering material. This arrangement retains a maximum of information on the arrival direction of the gamma-ray together with a sufficient total amount of high-Z material to provide a reasonable pair conversion efficiency. Further, once the pairs are formed, the plates may be used as scattering cells to obtain information on the electron momentum and hence the pair energy and arrival direction.

The entire chamber is hermetically sealed within a stainless steel cylindrical container with a hemispherical dome. The spark gas is confined within this shell which is designed to withstand pressure differentials of up to at least two atmospheres.

The high voltage pulsers, magnetic core trays, central scintillator light pipe, and the sense amplifier and shift register circuits used in the readout are mounted on the sides of the detector. The readout electronics are placed outside the sealed shell containing the spark chamber.

5. Coincidence - anticoincidence system

The spark chamber is energized whenever a coincidence telescope consisting of a thin scintillator and a Cerenkov counter detect the passage of a charged particle while a surrounding plastic guard scintillator detects nothing, denoting a neutral particle which interacts within the chamber.

The central Pilot B scintillator is viewed by an RCA C-7151H photomultiplier from one edge through a light pipe made from six strips of plexiglas which are heated and individually formed into a right angle elbow then bonded to the scintillator.

The Cerenkov radiator is a 2.5 cm thick disc of plexiglas blackened on top to discriminate against upcoming cosmic ray albedo and viewed from below by a 12.7 cm diameter RCA 2065 phototube.

The bell-shaped Pilot B anticoincidence dome, which is loosely covered with aluminum foil before a light seal of black epoxy is applied to the surface, is viewed by six-gain-matched photomultipliers mounted on the bottom ring. The output charges are summed to provide the anticoincidence signal. The loss of one of these photomultipliers, whose power supplies are independent, does not jeopardize the anticoincidence function.

A block diagram of the coincidence circuit is shown in Fig. 9. As can be seen from this diagram, a coincidence signal is obtained when the $\bar{A} B C$ condition is satisfied.

The 100 nanosecond delay seen in Fig. 9 is incorporated because of the large delay time inherent in the Cerenkov tube. The width of the gate is likewise made sufficiently large to avoid problems of transit time jitter in the Cerenkov tube and yet small enough to greatly reduce chance coincidences. The coincidence defeat conditions are merely incorporated as convenience for calibration and checkout of the coincidence telescope. The thin scintillator and Cerenkov tube are calibrated on ground level cosmic muons and when placed in coincidence provide excellent separation of signal from noise for relativistic singly ionizing particles.

6. The high voltage pulser

The modules of the detector are divided into sets of two which are driven by E. G. and G. type KN-2 Krytrons which in turn are driven by an avalanche transistor circuit common to eight Krytrons as shown in Fig. 10. Each module has

its own discharge capacitor to minimize problems of energy robbing between modules. The 2N2087 avalanche transistors provides a fast 800 volt trigger pulse to the grid of each Krytron. A 300 volt converter supplies both the avalanche circuit and a 150 microampere "keep-alive" current for each KN-2. The latter serves to reduce the delay time between the application of the coincidence trigger and the firing of the Krytron to about 50 nanoseconds with a rise time on the plate of about 15 nanoseconds. The total delay from the time of charged particle passage to the formation of the spark is about 300 nanoseconds. To minimize interaction between the high voltage circuits and the low level circuits, the grounds are separated by 10^3 ohms. In addition all high current grounds use large diameter buss wire to maintain low inductance.

It has been found that no clearing field is necessary for this application of the spark chamber. The mean time between charged particle passage through the detector is several milliseconds at balloon altitudes. On this time scale recombination and impurity attachment are quite sufficient to clear out the residual ions.

The limited lifetime of Krytron tubes which appears to be primarily associated with the keep-alive current rather than the number of pulses makes them unsuitable for long experiments on a satellite. The approach of using a spark gap in the high voltage pulser is being investigated and preliminary results show that both the size limitation and the lifetime problem can be overcome and that a suitable high voltage pulser can therefore be built.

7. On-board data handling system

The data system consists of a buffered memory readout system, a house-keeping data handling system and a tape multiplexer and recorder. Each of the

30 wire grid decks contains 256 cores and the two forty-five degree grids 128 cores each for a total of 7936 cores to be read out. Each core is threaded by three wires: the spark wire, which carries current to set the core; a reset wire, which threads 32 cores, one per module, and carries current to reset the core; and a sense wire, which threads all 256 cores of one module, and senses cores changing state. The "three-dimensional" readout scheme consisting of 16 current sources, 16 grounding circuits, and 32 sense amplifiers is depicted in Fig. 11.

Each of the current sources provides 0.8 ampere, one microsecond pulses through one of sixteen columns of cores indicated by the grounding circuit select system. By selecting one current pulser and one grounding circuit the contents of a column of thirty-two cores are detected by their associated sense wires. These sense wires are in turn transformer coupled to thirty-two sense amplifiers which detect the 0.5 volt output pulses from the set cores as they are reset. The outputs of the sense amplifiers are transferred into a thirty-two bit shift register.

The readout is initiated by an output from the anticoincidence-coincidence telescope. A millisecond delay allows the spark transients to die away, then all scalers are set to zero, the shift register is cleared, the first reset wire is pulsed and the outputs of the first column of cores is loaded into the shift register. As depicted schematically in Fig. 12, shift pulses are counted until a set core is found at which time counting and shifting are inhibited until the core address (which corresponds to the number of shift pulses since the readout cycle began) is recorded. After thirty-two shift pulses, the second reset wire is pulsed and the outputs of the second column of cores is stored in the shift

register. The process iterates until all cores are examined. The shifting occurs at a rate of 12,288 cores per second, and on the average an additional $1/42$ of a second is required to record the address of a set core. Hence, the total time required to readout an event in which n cores are set is a maximum of $(.67 + n/42)$ seconds. In a typical event in which about 120 cores are set, 3.5 seconds would be required to read out and record the event. The readout rate is limited by the balloon tape recorder and could easily be substantially increased if another data storage system were available.

During the readout time, the chamber is inhibited against further coincidence signals until the entire core array has been read out and recorded. Thus, readout time represents dead time for the chamber. Since the neutral particle event rate at ceiling is about one count every 6.5 seconds, the live time is about 65 percent of the elapsed time. This value is somewhat low but acceptable.

It is also desirable in aiding the analysis to record other peripheral data herein called "housekeeping" data. The housekeeping system, as well as some aspects of the electronics not discussed here, has been described previously by Ehrmann¹³). The method of scientific analysis of the data will be discussed in a later article.

8. Concluding remarks

The excellent operation of this chamber, both on balloon flights and after environmental tests, together with an encouraging preliminary study has lead us to begin the design of a larger spark chamber module for space use, with inside dimensions of approximately $1/2$ meter square. It appears that a chamber of this size can be built in such a way that it can pass the tests associated with the

launch and space environment and operate properly for about a year. The severe shock and vibration encountered during the launch phase make it difficult to build a chamber with many large thin plates that is larger than this size even if the plates are not active electrical elements, but larger experiments could be composed of clusters of the $1/2 \text{ m} \times 1/2 \text{ m}$ chambers. Thus, there seems every reason to believe that digitized spark chambers can be built to satisfy the requirements of even very large space experiments.

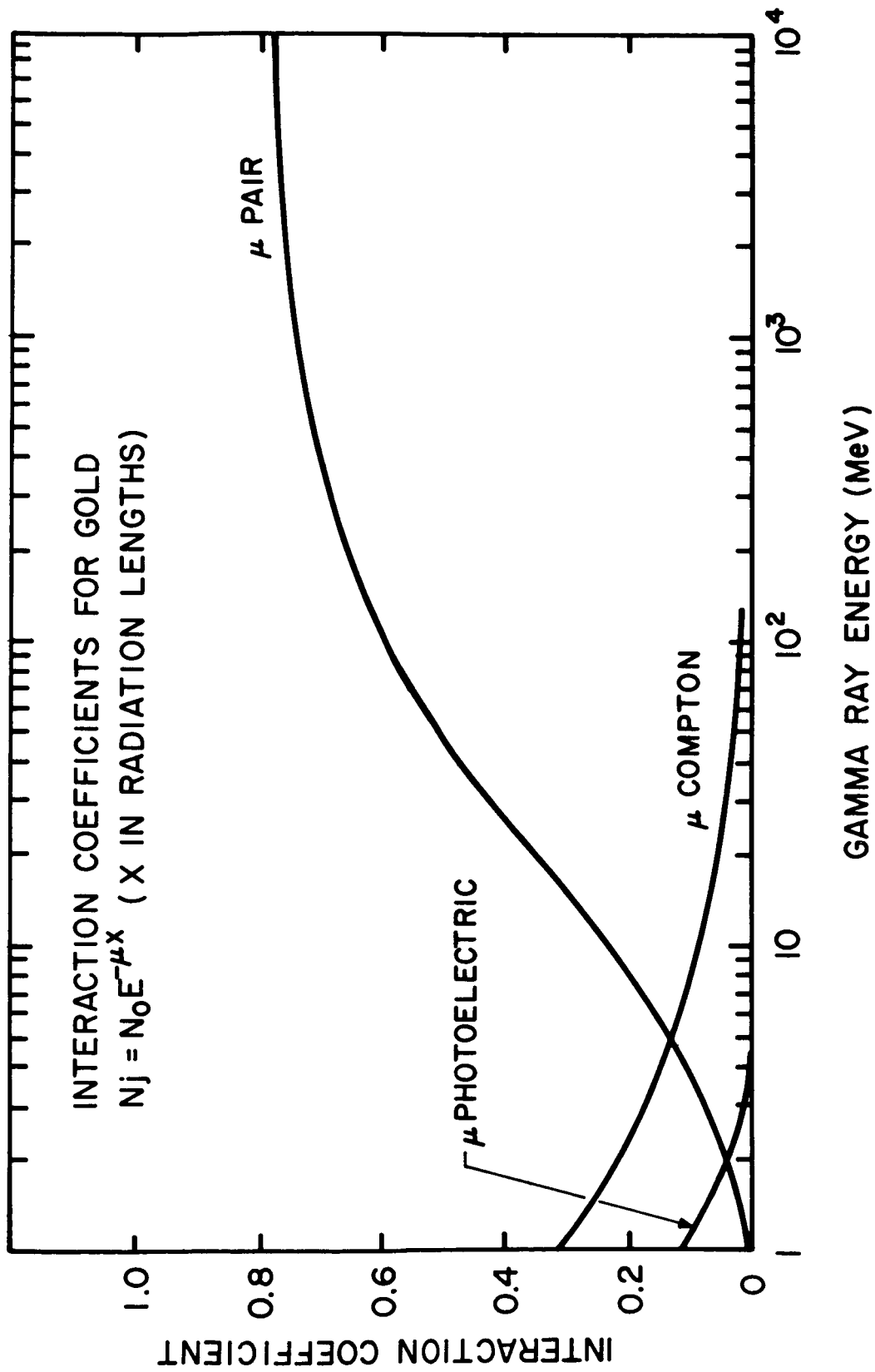
References

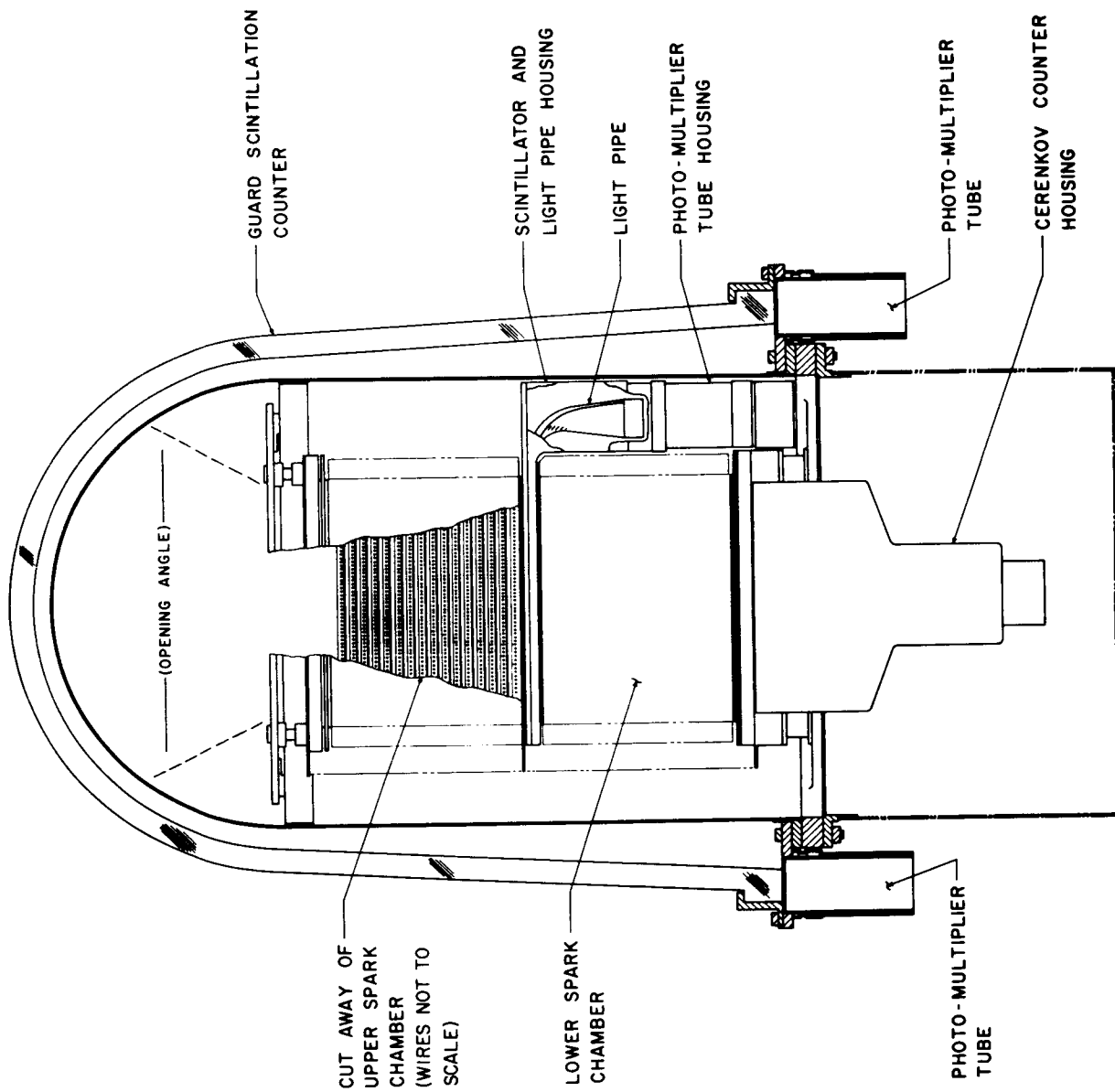
- ¹⁾ J. A. Earl, Phys. Rev. Letters, 6, (1961) 125.
- ²⁾ G. Svensson, Arkiv För Fyski, 13, (1958) 347.
- ³⁾ A. Bracessi and M. Ceccarelli, Il Nuovo Cimento, 17, (1960) 691.
- ⁴⁾ J. Klarmann, Il Nuovo Cimento, 24 (1962) 540.
- ⁵⁾ C. E. Fichtel and D. A. Kniffen, J. Geophys. Res., 70, (1965) 4227.
- ⁶⁾ G. M. Frye, F. Reines, and A. H. Armstrong, J. of Geophys. Res. 71, (1966) 3119.
- ⁷⁾ F. Krienen, Nuclear Instruments and Methods 16, (1962) 262.
- ⁸⁾ F. Krienen, Nuclear Instruments and Methods 20, (1963) 168.
- ⁹⁾ J. Fischer, G. B. Collins, and W. A. Higinbotham, International Symposium on Nuclear Electronics, Paris, (1963).
- ¹⁰⁾ J. O'Conner, to be published.
- ¹¹⁾ F. Schneider CERN AR/Int., (1963) GS/63-9.
- ¹²⁾ M. J. Druyvesten and F. M. Penning, Rev. Mod. Phys., 12, (1940) 87.
- ¹³⁾ C. H. Ehrmann, Proceedings of the 13th Nuclear Science Symposium, Transactions on Nuclear Science NS-13, (1966) 503.

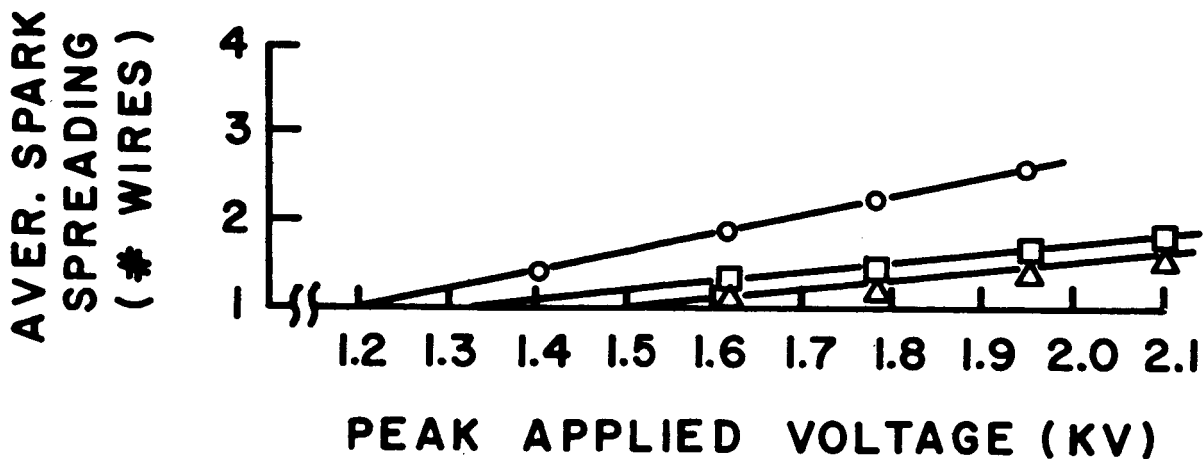
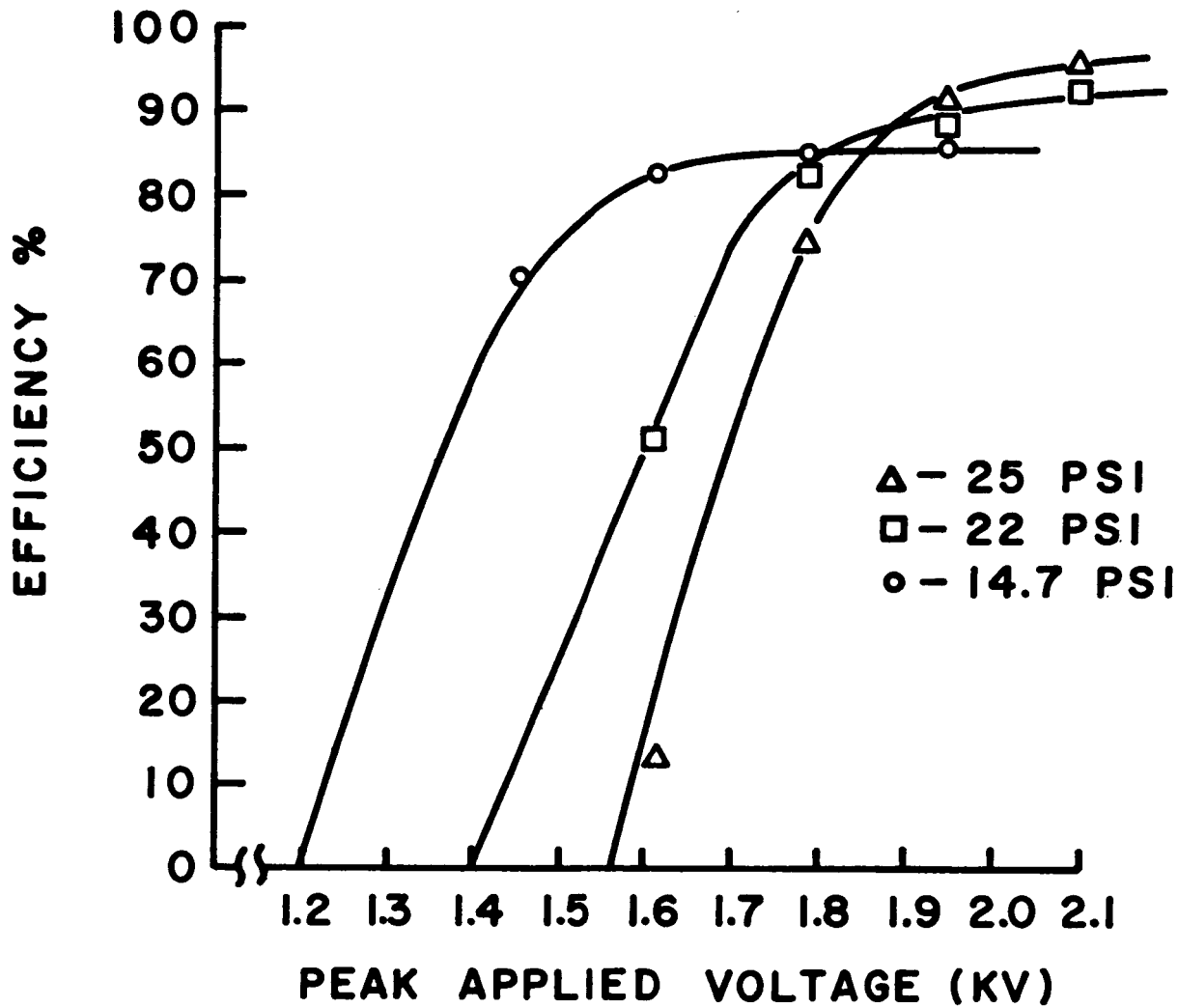
Figure captions

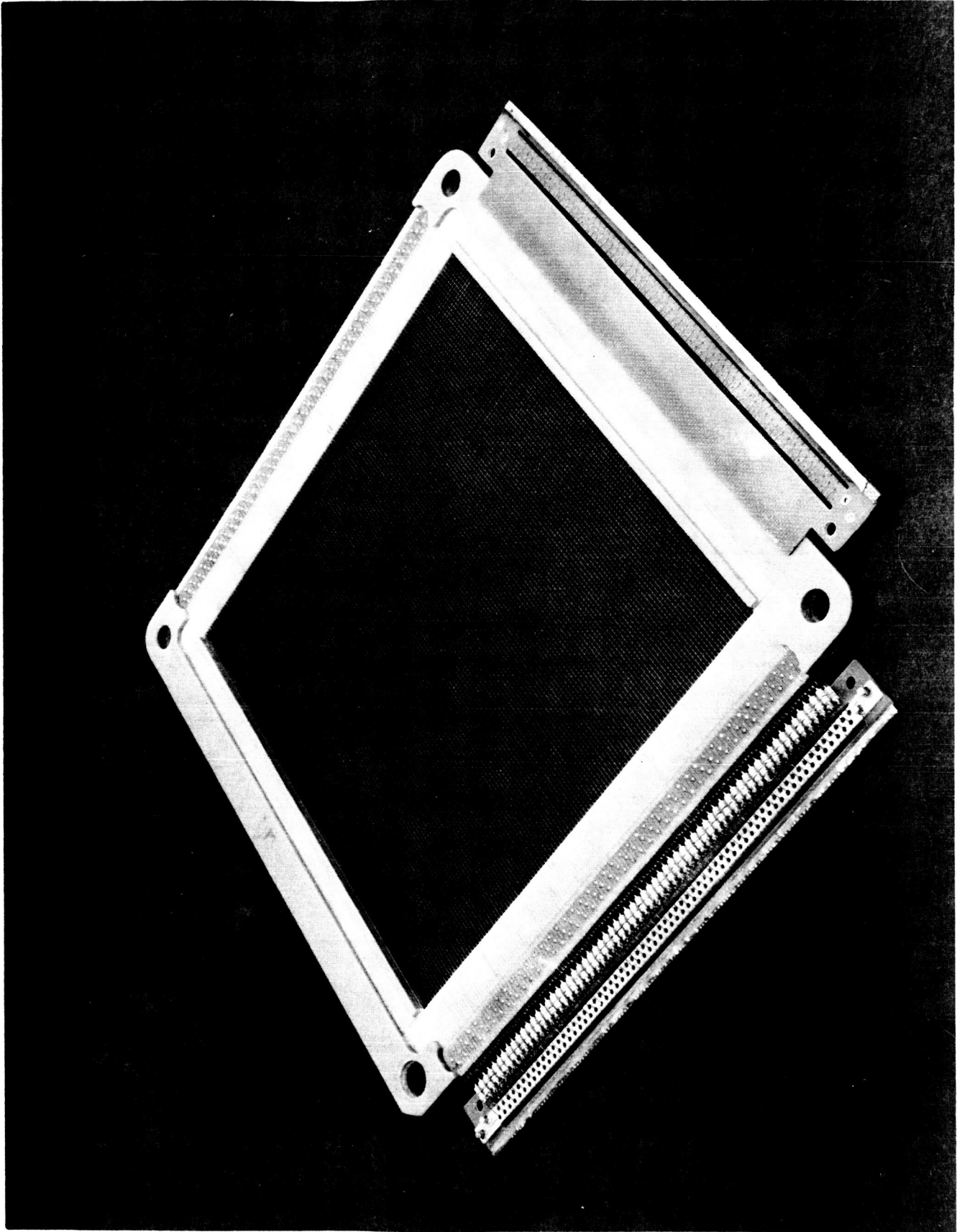
- Fig. 1. A plot of the interaction coefficients for electromagnetic interactions in gold, where the distance traveled, x , is measured in radiation lengths.
- Fig. 2. A diagrammatic representation of the assembled gamma-ray digitized spark chamber.
- Fig. 3. A photograph of a single spark module in which two orthogonal wire grid planes form the two spark electrodes. There are 30 such modules in two sets of 15 in the assembled detector. Circuit boards along two orthogonal sides contain the ferrite cores and the resistors, R_w , discussed in the text.
- Fig. 4. Results of single-module tests on cosmic-ray ground level muons. $R_w = 0$. The upper curve represents single track efficiency, the lower curve the average number of adjacent cores set per single spark, plotted as a function of applied voltage, V_A . $R_w = 0$, $R_\ell = 22$ ohms, $R_0 = 150$ ohms, $C_0 = 1000$ pf, $C_p = 175$ pf. Gas mixture (by pressure): 89.5% neon, 9.0% helium, 1.0 percent argon, 0.5% ethanol.
- Fig. 5. Same as Fig. 4 for $R_w = 100$ ohms. Other parameters and gas mixture are the same.
- Fig. 6. (a) Equivalent charging circuit for a typical module of the digitized spark chamber, neglecting stray inductances.
(b) Equivalent discharge circuit with the approximation that $R_\ell \ll R_w$.

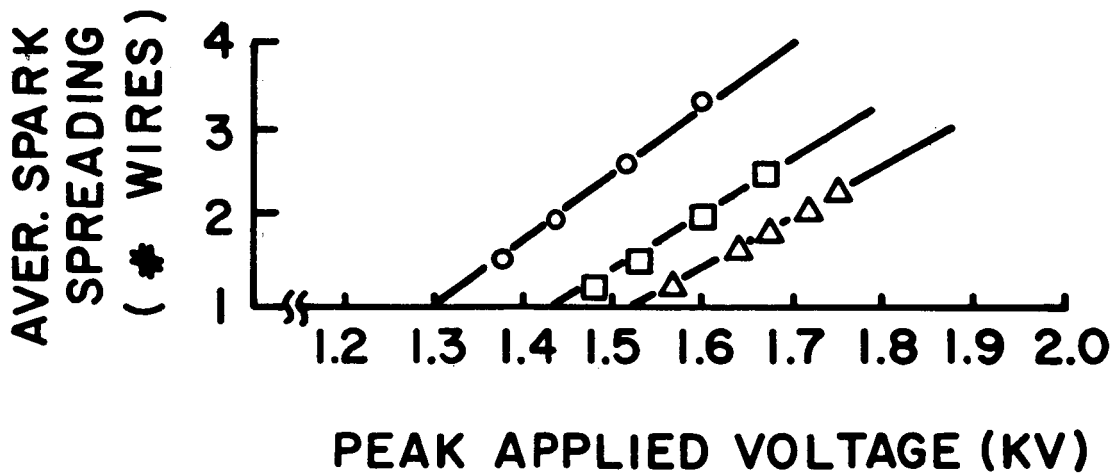
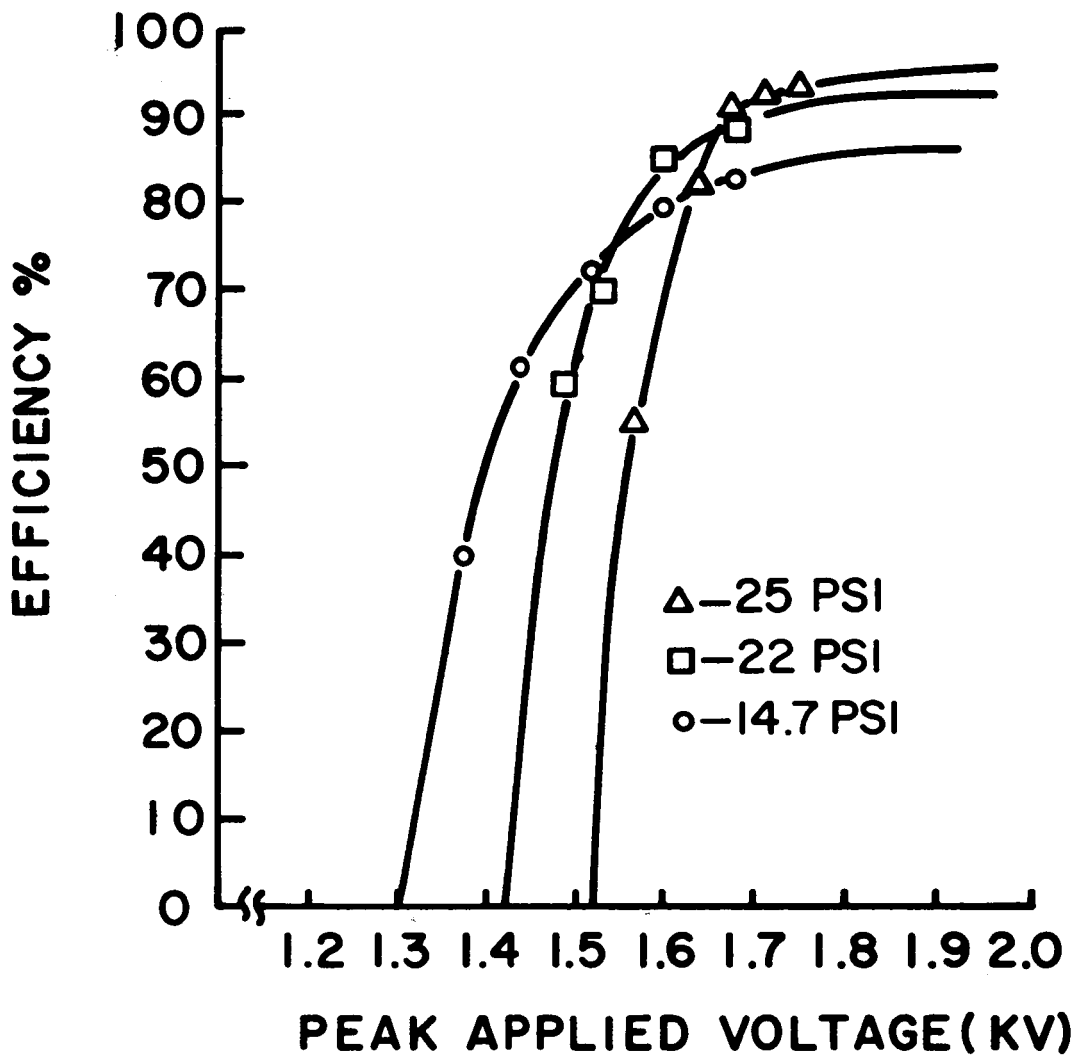
- Fig. 7. Calculated pulse shapes of the grid voltage (V_p) as a function of time for the equivalent circuit shown in Fig. 6 (a).
- Fig. 8. A photograph of the assembled chamber without metal cover or anti-coincidence dome.
- Fig. 9. A block diagram of the coincidence circuit.
- Fig. 10. A schematic diagram of the high-voltage pulser circuitry. Each Krytron serves two modules. There are two such pulsers in the assembled chamber, housed in hermetically sealed containers.
- Fig. 11. A three-dimensional representation of the core readout electronics.
- Fig. 12. A functional diagram of the core readout electronics.



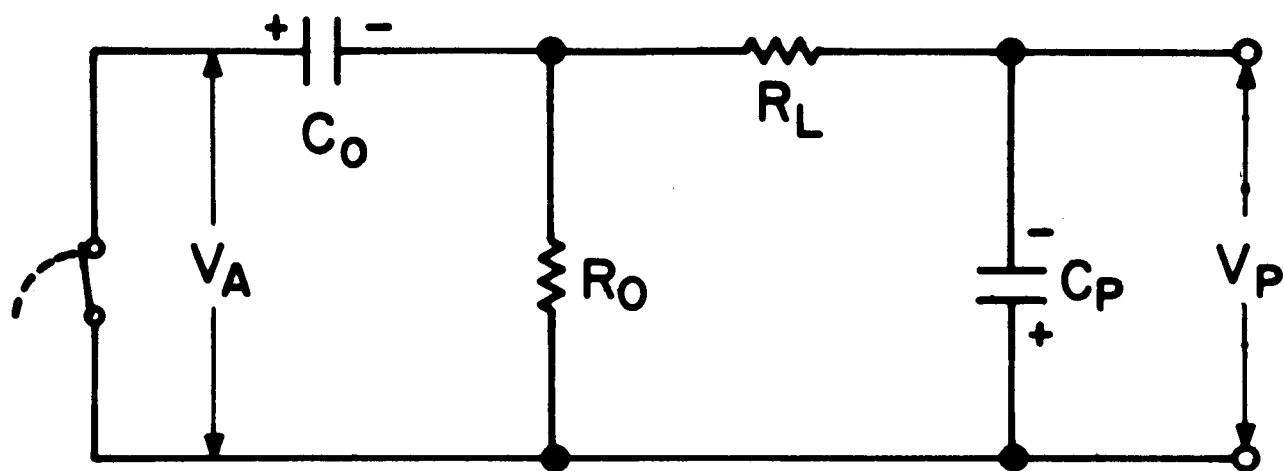






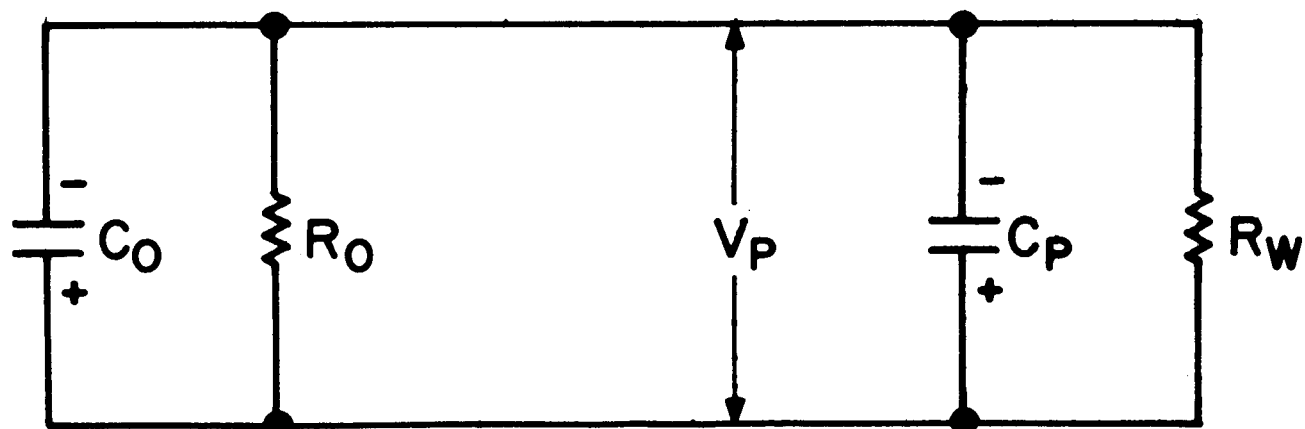


SIMPLIFIED CHARGING CKT.



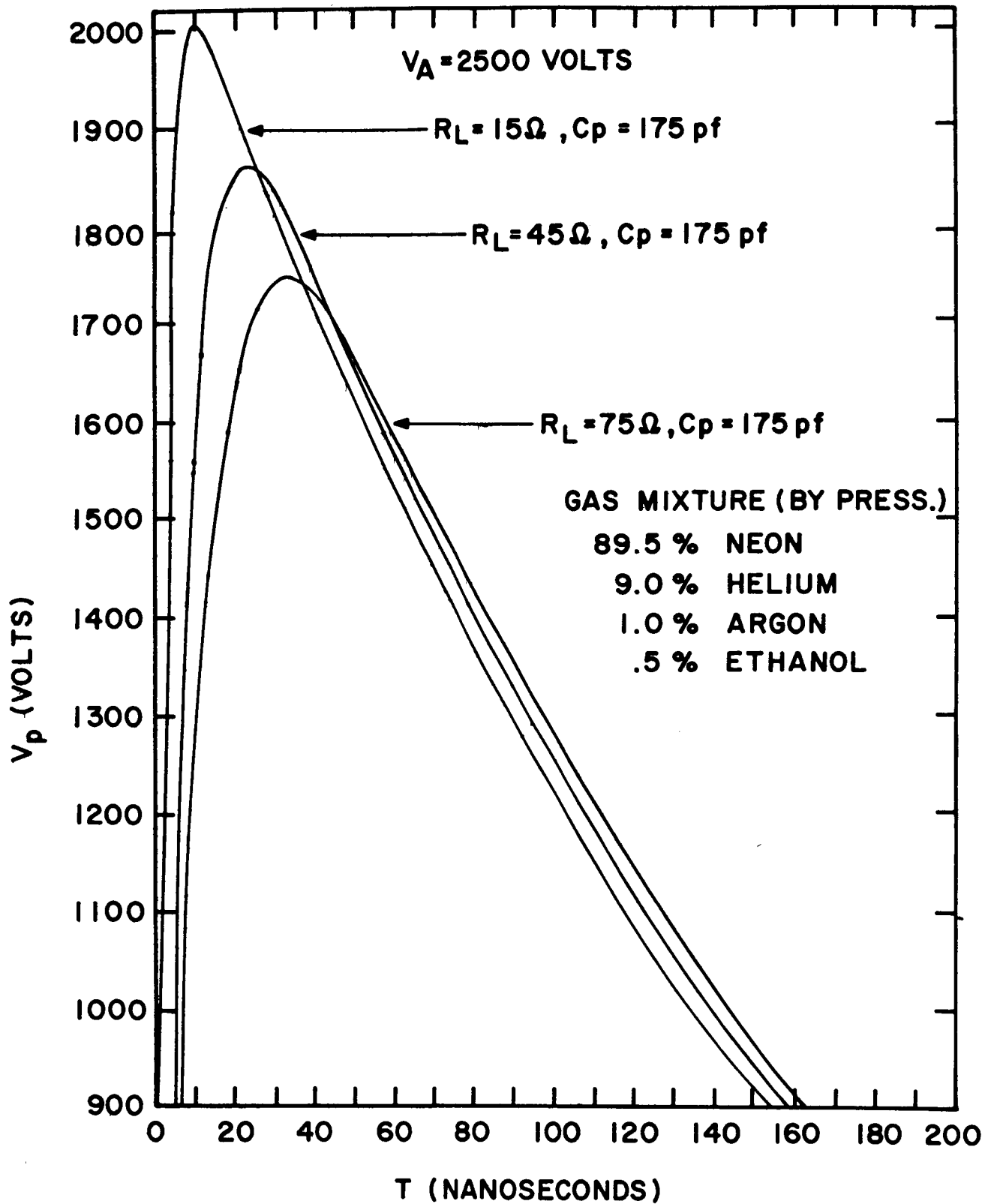
(a)

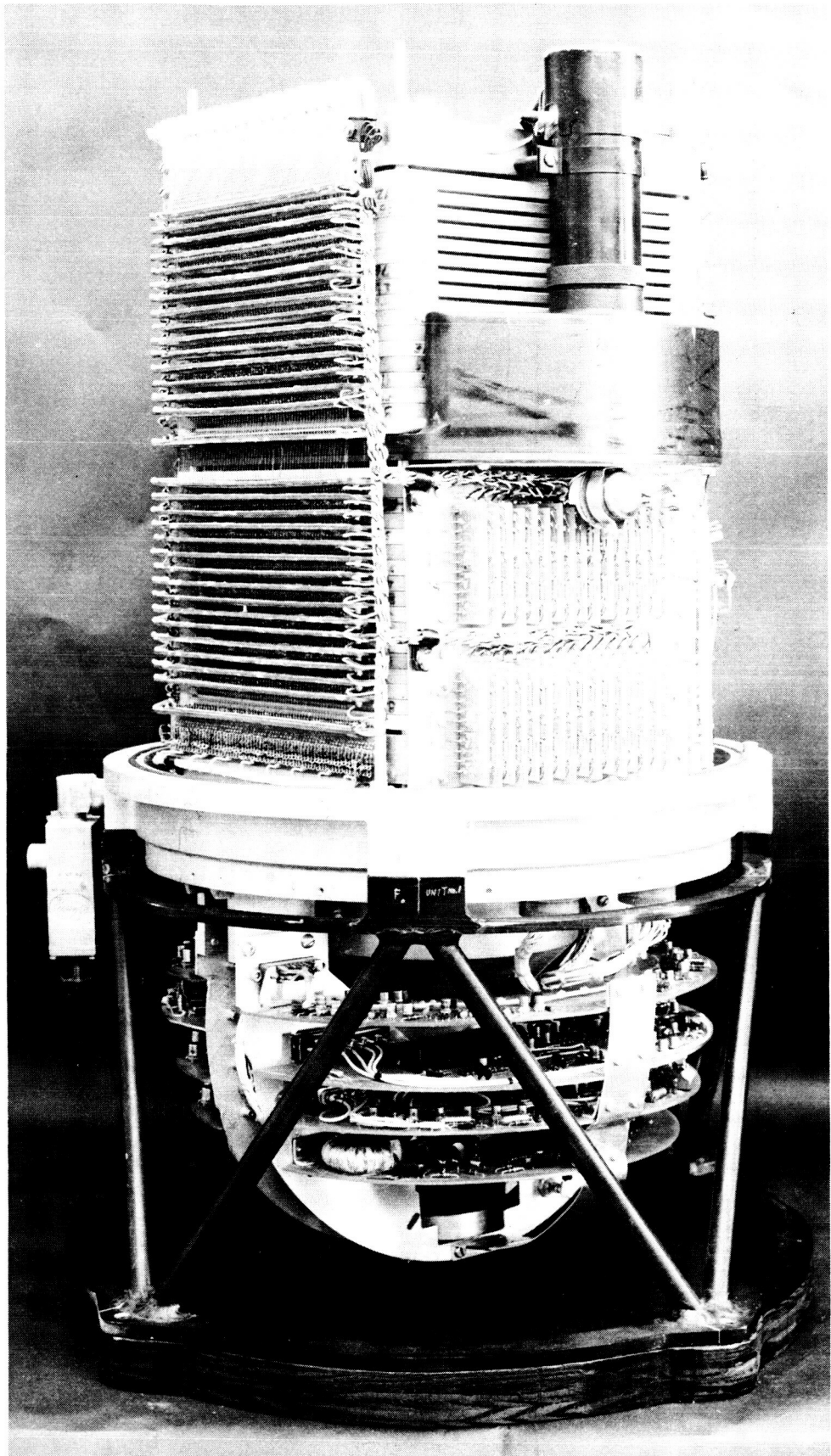
SIMPLIFIED DISCHARGE CKT.

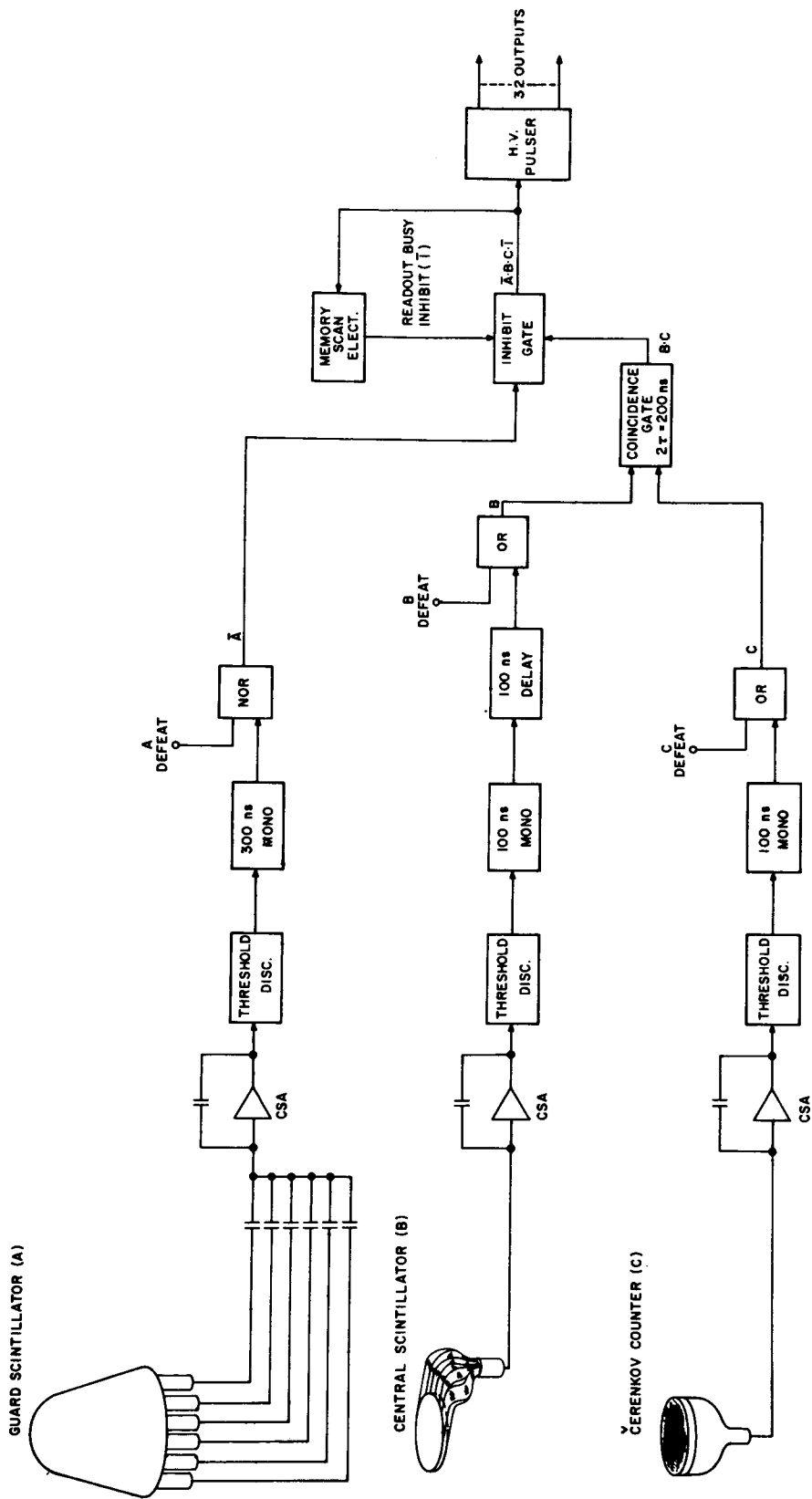


$$R_L \ll R_W$$

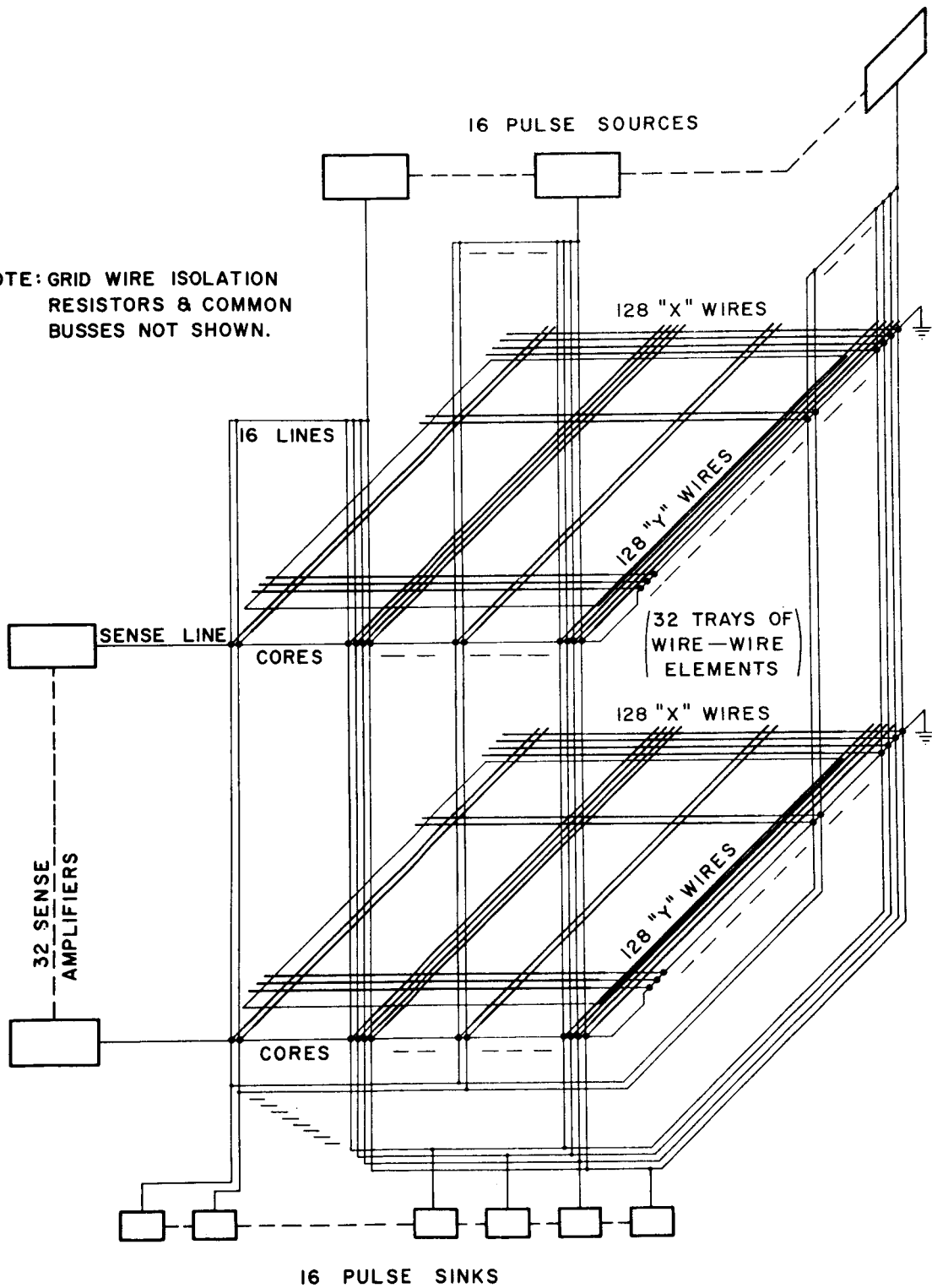
(b)

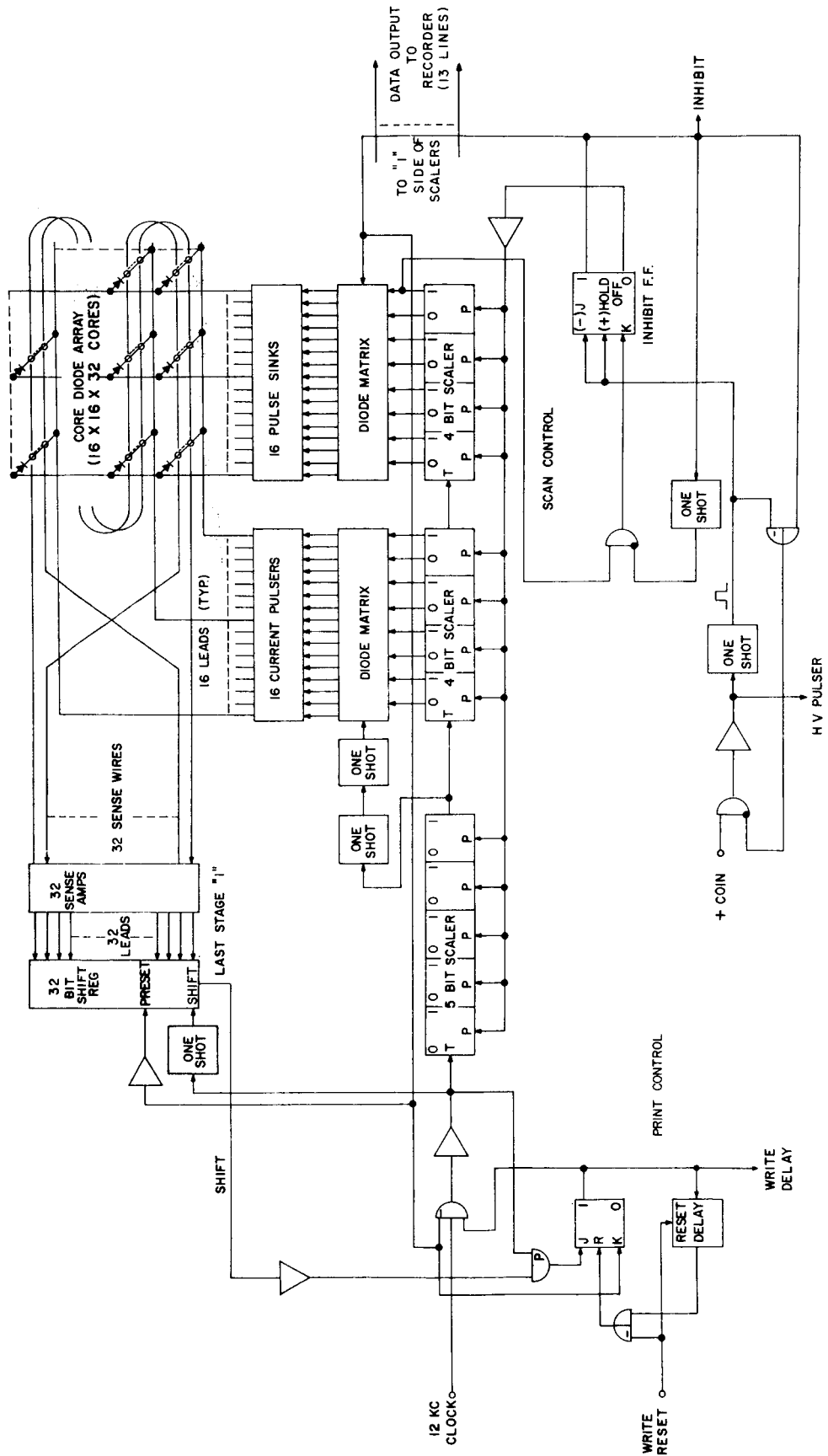






NOTE: GRID WIRE ISOLATION
RESISTORS & COMMON
BUSSES NOT SHOWN.





SCAN ELECTRONICS BLOCK DIAGRAM